CONTROL-ORIENTED MODELING AND ANALYSIS OF AERO-THERMO-ELASTIC-PROPULSION HYPERSONIC VEHICLE

Jin Xiao, Ping Lin
School of Astronautics, Beihang University, Beijing 100191, China
xj0618@163.com;saofbuaalp@163.com

Keywords: *hypersonic vehicles; aerodynamic configurations; flight dynamics; aerodynamic heating; mathematical models*

Abstract

A parametric configuration generation system is developed for wave-rider air-breathing hypersonic vehicle. Inviscid flow aerodynamic forces and viscosity resistance caused by aerodynamic heating are calculated with engineering method. Based on thermal-flexible structure assumption of airframe and scramjet engine model, a multi-field coupling model with aerodynamic / thermal / structure /propulsion is obtained and the table data of aerodynamic forces and thrust have been curve fitted for control law design. Simulation analysis shows that this model reflects the complicated strong coupling between aerodynamic, thermal, structure, and propulsion in hypersonic flight. The engineering calculation method is fast and convenient with acceptable accuracy. The obtained multi-field model has good trim flight performance and suitable for flight control law design and analysis.

1 Introduction

The next generation air-breathing hypersonic vehicle widely utilizes scramjet-powered, lifting body, and wave-rider aero-dynamics layout. In order to enhance the thrust to weight ratio, the extensive use of lightweight materials lead the flexible structures have low natural frequencies. In addition, under the conditions of high Mach, there will be highly non-linear fluid dynamics, and high temperature physical and chemical properties caused by the flow of energy. Thus, the vehicle's aerodynamic calculations have a great deal of uncertainties.

The above-mentioned characteristics of air-breathing hypersonic vehicle bring many challenges for flight control system design, such as: serious coupling between aerodynamic / thermal / structure / propulsion, large time-varying of flight parameters, model uncertainty, unstable / non-minimum phase dynamics and control constraints etc[1,2].

As early as the 1990s, some U.S. scholars had been carried out related researches. 1986-1995, for X-30, the group led by David K. Schmidt and Martin R. Waszak, derived the coupling dynamic equations of flexible vehicle based on Lagrange equations and principle of virtual work [3-5]. In 1994, Frank R. Chavez and David K. Schmidt established a scramjet / aero-elastic coupled model of flexible hypersonic vehicle [6]. 2005-2007, on the basis of above studies, Michael A. Bolender and David B. Doman conducted a longitudinal plane flexible body dynamics model, aerodynamic model and scramjet model for the wave-rider hypersonic vehicle [7, 8]. At the same time, Trevor Williams, Oscar Morataya and Michael A. Bolender conducted aerodynamic heating, and heat transfer modeling and analysis for X-43C [9-11]. 2008-2010, Armando A. Rodriguez and Jeffrey J. Dickeson, carried out the air-breathing hypersonic vehicle body control / propulsion integration model design and analysis.

In this paper, first a parameterized configuration is established for wave-rider air-breathing hypersonic vehicle. Then by using hypersonic inviscid flow theory and viscous drag engineering calculation method, aerodynamic forces are calculated. Combined with flexible body assumptions and simplified

scramjet model, a multi-field coupling model is formed with the integration of aerodynamic, structural, thermal, and propulsion. The polynomial fitting formulas of aerodynamic and thrust are given. Next, the work envelope of scramjet and trim flight capacity of this control model are analyzed. Finally, the pole-zero point analysis and the mode sensitivity analysis were used to analyze the dynamic characteristics.

2 Parametric modeling and aerodynamic calculated with engineering method

2.1 Parametric configuration modeling

Parameterized configuration approach determines the geometric configuration of AHV by setting a number of body, wings and other parameters. Configuration modification can be achieved easily through resetting corresponding parameters in the program. It avoids redrawing vehicle configuration and re-meshing the flow field which are necessary for methods based on CFD software. Therefore it is convenient in the preliminary design stage.

AHV model in this paper refers to the shape of X-43C and the parameters are shown in table 1.

Table 1 Configuration parameters

Variable	Value	Meaning
L	30.48m	Body length
W	9.144m	Body width
H	3.2036m	Body height
W_E	6.096m	Engine width
Y_E	-2.3347m	Longitudinal coordinate of engine bottom
D_{1F}	3°	First wedge inclination of forebody
X_{1F}	0.47m	Axial relative coordinate of intersection of wedge 1
X_N	0.8m	Axial relative coordinate of scramjet engine and afterbody
D_{ON}	8.5142°	Inclination of outside part of afterbody
X_{1E}	0.3075m	Axial relative coordinate of the front and rear point of engine bottom
X_{2E}	0.67m	
L_{WR}	8.9369m	Chord length of wing root
L_{WT}	3.6576m	Chord length of wing tip
L_{WS}	3.048m	Wing length
T_S	60°	Sweep angle of leading edge
C_W	0.03m	Relative thickness

The 3D geometric model of vehicle is obtained by using scientific graphics software, shown in Fig.1 and Fig.2.

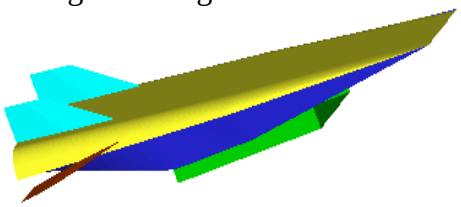

Fig. 1 AHV Three-Direction Configuration

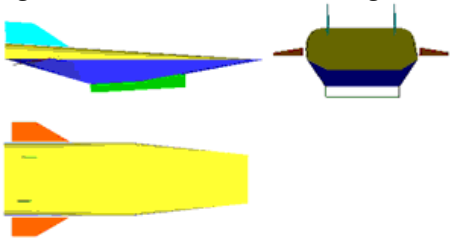

Fig. 2 AHV Three-Direction View

2.2 Aerodynamic calculated with engineering method

In the first state or concept research of vehicle design, aerodynamic prediction is a very important work and usually costs much for the wind tunnel experiments. As the development of computational fluid dynamics, there are a lot of numerical methods for aerodynamic prediction. However, these methods often require high performance computers with long time circle. Then the engineering method is still an effective tool for rapid aerodynamic calculation to save time and cost.

The processes of aerodynamic engineering calculate method is as follow:

First, the surface panel of vehicle is chosen in sequence, and then the properties (area of surface panel, mass center position, external normal direction etc.) and pressure coefficient of each surface panel are calculated. Next, the aerodynamic on the body axes coordinate system is obtained from vector sum of distributed force of all the surface panels and finally converted to air axes coordinate system.

For the engineering method, the pressure coefficient of each panel is calculated with the Dahlem-Buck method and the Prandtl-Meyer method [12, 13]. The aerodynamic coefficients of vehicle can then be obtained by summing up the

pressure coefficients of all the panels on the surfaces of vehicle.

The Dahlem-Buck method is used for the windward sides of vehicle body:

$$C_p = C_{pD} \cdot \frac{C_{pcone}(Ma \le 20)}{C_{pcone}(Ma = 20)} \tag{1}$$

$$C_{pD} = \begin{cases} [\frac{1}{\sin^{3/4}(4\delta)} + 1]\sin^2\delta & 0 \le \delta \le 22.5° \\ K\sin^2\delta & \delta > 22.5° \end{cases} \tag{2}$$

$$C_{pcone}(Ma) = 2e^{\xi}\sin^2\delta \tag{3}$$

Where, Cp is pressure coefficient, Ma is Mach, K is fitted as the functions of impact angle δ respectively for the body, wings, rudder and elevators as follow:

$$K = 2.38 + 0.03792\delta - 0.002521\delta^2 + 0.00004583\delta^3 + 2.917\times10^{-7}\delta^4 \tag{4}$$

$$K = 3.24 - 0.08867\delta + 0.002775\delta^2 - 4.333\times10^{-5}\delta^3 + 2.5\times10^{-7}\delta^4 \tag{5}$$

$$K = 1.15 + 0.004179\delta + 0.0009958\delta^2 - 4.166\times10^{-6}\delta^3 + 4.166\times10^{-8}\delta^4 \tag{6}$$

The Prandtl-Meyer method is used for the leeward sides of vehicle body:

$$C_p = -\frac{\gamma_0 + 1}{2}\delta^2 \left\{ \sqrt{1 + [\frac{4}{(\gamma_0 + 1)Ma_\infty \delta}]^2} - 1 \right\} \tag{7}$$

Where γ_0 is atmospheric specific heat ratio and here is valued as 1.4.

In addition, the tangent-cone method is used for the windward sides of wings:

$$C_p = \frac{4\sin^2\theta(2.5 + 8\sqrt{Ma_\infty{}^2 - 1}\cdot\sin\delta)}{1 + 16\sqrt{Ma_\infty{}^2 - 1}\cdot\sin\delta} \tag{8}$$

The shock expansion wave method is used for the leeward sides of wings:

$$C_p = \frac{2}{\gamma_0 Ma_\infty{}^2}\left[\left(1 + \frac{\gamma_0 - 1}{2} Ma_\infty \sin\delta\right)^{\frac{2\gamma_0}{\gamma_0 - 1}} - 1 \right] \tag{9}$$

Where θ is surface inclination.

2.3 Aerodynamic Heating Effect

When vehicle flights in high altitude with high Mach, there is serious aerodynamic heating on the surface, and it will generate viscous drag which affects the size of drag. The reference temperature method has been adopted to calculate the viscous drag caused by aerodynamic heating.

Eckert reference temperature method is applicable to laminar flow and turbulent flow. And it has been widely used in engineering design. In this method, reference temperature T^* is defined as:

$$\frac{T^*}{T_e} = 0.5 + 0.5\frac{T_w}{T_e} + 0.22\left(\frac{T_r}{T_e} - 1\right) \tag{10}$$

Where T_e is the temperature of boundary layer edge, T_w is wall temperature, T_r is recovery temperature.

When reference temperature is obtained, we can calculate relevant airflow parameters.

Coefficient of viscosity at the reference temperature is:

$$\frac{\mu^*}{\mu_e} = \left(\frac{T^*}{T_e}\right)^w \tag{11}$$

Generally, $w = 0.75$ and air density at the reference temperature is:

$$\rho^* = \frac{p_e}{RT^*} \tag{12}$$

Thus, the Reynolds number at the reference temperature is:

$$Re_e^* = \frac{\rho^* V_e x}{\mu^*} \tag{13}$$

Viscous drag coefficients are obtained in the case of laminar and turbulent flow respectively.

Laminar flow:

$$C_f^* = \frac{0.664}{\sqrt{Re_e}}\left(\frac{T^*}{T_e}\right)^{\frac{w-1}{2}} \tag{14}$$

Turbulent flow:

$$C_f^* = \begin{cases} \dfrac{0.0592}{\sqrt[5]{Re_e^*}} & Re_e \le 10^7 \\ 0.37\cdot(\lg Re_e^*)^{-2.584} & Re_e > 10^7 \end{cases} \tag{15}$$

For the air-breathing hypersonic vehicle model, the vehicle's total viscous drag coefficient is the sum of the viscous drag coefficient by surface generated by the following equation:

$$C_f^* = C_{f\,upsurface}^* + C_{f\,forebody}^* + C_{f\,eng}^* + C_{f\,wing}^* \tag{16}$$

Therefore, the vehicle's total axial force coefficient C_A is the sum of wave drag coefficient C_{AP} and the total viscous drag coefficient:

$$C_A = C_{AP} + C_f^* \tag{17}$$

For the vertical flight plane, axial force coefficient C_A and normal force C_N are usually transferred into the lift coefficient C_L and drag coefficient C_D, by following equations:

$$C_L = C_N \cos\alpha - C_A \sin\alpha$$
$$C_D = C_A \cos\alpha + C_N \sin\alpha \quad (18)$$

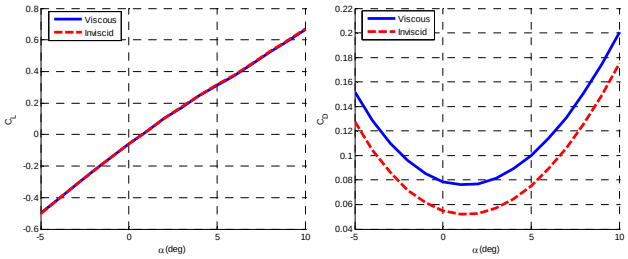

Fig. 3 contrast of C_L、C_D against AOA between Viscous and Inviscid

Fig.3 shows that the impact of temperature on the aerodynamic force is mainly reflected in the aerodynamic drag, and the viscous drag coefficient with angle of attack (AOA) is slightly different. For the minimum AOA, the change caused by the viscous drag coefficient to the total drag coefficient reaches the maximum value, that is 38%. Thus the viscous drag generated by the boundary layer temperature on the aerodynamic forces cannot be ignored.

3 Integrated modeling of flexible body and propulsion

3.1 Thermo elastic assumptions of the body

In order to reduce the amount of simulation and without losing the authenticity, in this paper, the vibration model of the fuselage is simplified as a single free-free Euler-Bernoulli beam.

Based on the above assumptions, the vibration displacement $w(x,t)$ is function of the axial coordination of body-axis and the time. By the beam bending theory, the non damping free vibration equation is as follow:

$$EI\frac{\partial^4 w(x,t)}{\partial x^4} + \tilde{m}\frac{\partial^2 w(x,t)}{\partial t^2} = 0 \quad (19)$$

Assuming that the solution has the form:

$$w(x,t) = \Phi(x)\eta(t) \quad (20)$$

Where $\Phi(x)$ is mode shape, $\eta(t)$ is generalized displacement coordinates of structure.

Then, Eq. (19) can be separated into two ordinary differential equations:

$$EI\frac{\mathrm{d}^4\Phi(x)}{\mathrm{d}x^4} - \omega^2\tilde{m}\Phi(x) = 0 \quad (21)$$

$$\frac{\mathrm{d}^2\eta(t)}{\mathrm{d}t^2} + \omega^2\eta(t) = 0 \quad (22)$$

Defining $a^4 = \omega^2\tilde{m}/(EI)$; Eq. (21) takes the form:

$$\frac{\mathrm{d}^4\Phi(x)}{\mathrm{d}x^4} - a^4\Phi(x) = 0 \quad (23)$$

The solution of Eq. (23) is:

$$\Phi(x) = A\sin ax + B\cos ax + C\sinh ax + D\cos ax \quad (24)$$

Apply the following boundary conditions:

$$\Phi''(0) = 0, \Phi'''(0) = 0,$$
$$\Phi''(l) = 0, \Phi'''(l) = 0 \quad (25)$$

The following frequency equation is obtained:

$$\cos a_i l \cosh a_i l = 1 \quad (26)$$

The solution of Eq. (26) is

$$a_i l = 4.73, 7.85, 10.99, 14.14, \ldots \quad (27)$$

Through a series of deformation, we can obtain the analytical solution of all vibration modes:

$$\Phi_i(x) = \sin(a_i x) + \sinh(a_i x) + \beta_i[\cos(a_i x) + \cosh(a_i x)] \quad (28)$$

Where the coefficient $\beta_i = \dfrac{\sinh(a_i l) - \sin(a_i l)}{\cos(a_i l) - \cosh(a_i l)}$.

Fig.4 shows the first four mode shapes of fuselage vibration.

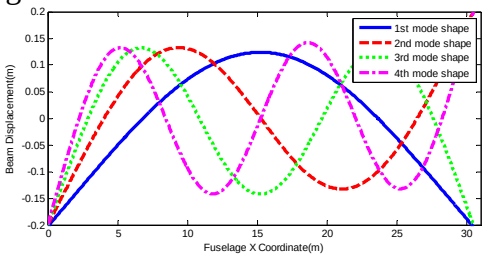

Fig. 4 Fuselage structure mode shape

The simplified inherent vibration frequency of the beam can be obtained by the following formula:

$$\omega_i = a_i^2\sqrt{\frac{EI}{m}} \quad (29)$$

Experiments show that the structural temperature changes also affect the properties of the material, thereby changing the natural vibration frequency of structure.

In Ref. [14], there are the Young's modulus data of aerospace titanium alloy variation with temperature. By unit conversion and data fitting, Young's modulus E of the titanium material is written as a function of temperature T in the form as follow:

$$E = 6.0822\times10^{10} - \frac{1.6422\times10^{10}}{463}(T-37)\ \ (\mathrm{kg/m^2}) \tag{30}$$

Based on the above assumptions of the beam, the structure vibration velocity of body vertical is superimposed to the speed of the stream:

$$V_x = V_\infty\cos\alpha\cos\beta, V_y = V_\infty\sin\beta, V_z = V_\infty\sin\alpha\cos\beta + w \tag{31}$$

Where V_∞ is the speed of the stream, and $w = \Phi(x)\dot{\eta}(t)$. α, β are AOA and sideslip angle separately.

The airflow impact angle of each surface element is as follow:

$$\delta^* = \arccos\frac{\boldsymbol{n}\cdot\boldsymbol{V}^*}{|\boldsymbol{n}|\cdot|\boldsymbol{V}^*|} - \frac{\pi}{2} \tag{32}$$

Where $\boldsymbol{V}^*$ is the flow velocity vector which includes the structure vibration velocity. The pressure coefficient distribution is obtained by the Mach and the revised impact angle of local air flow. Then we can get a more realistic aerodynamic force and moment coefficients. In addition, the structure vibration displacement at the elevator stalled position will also lead to the emergence of an additional fin deflection angle:

$$\Delta\delta_e = \arctan[\Phi'(x_{\delta_e})\eta(t)] \tag{33}$$

Therefore, the real fin deflection angle is:

$$\delta_e^* = \delta_e + \Delta\delta_e \tag{34}$$

Typically, the vibration mode number of the continuum structure is infinite, but in this paper, the first order mode whose frequency closest to the rigid body motion is taken.

3.2 Scramjet modeling

When the vehicle flight with hypersonic in the atmosphere, the most reliable and economical propulsion system is a scramjet. Ref. [15] proposed a modeling approach of scramjet properly seize the vehicle airframe / propulsion coupling characteristics. In this paper, a similar approach is applied for scramjet modeling. Scramjet engine are divided into five parts with different function (shown in Fig.5): inside compression section, outside compression section, combustion section, within expansion section and outside expansion section. Then, the theory of supersonic combustion propulsion is used to calculate each part and finally engine thrust is got. Table 2 shows label instructions of each part [16].

According to momentum theorem [17], the thrust of the scramjet engine is:

$$\mathrm{T} = \dot{m}_a(V_a - V_0) + (p_9 - p_0)A_9 - (p_2 - p_0)A_1 \tag{35}$$

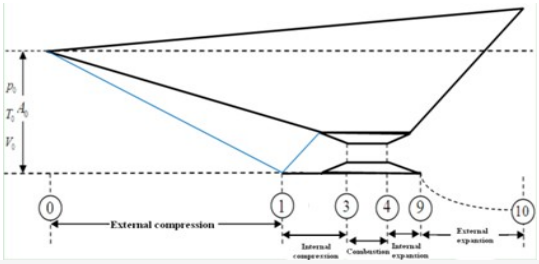

Fig. 5 Scramjet model

Table 2 Scramjet label illustration

Lable	Illustration
0	Undisturbed or freestream conditions
	External compression begins
1	External compression ends
	Internal compression begins
	Inlet or diffuser entry
3	Inlet or diffuser exit
	Internal compression ends
	Burner or combustor entry
4	Burner or combustor exit
	Internal expansion begins
	Nozzle entry
9	Internal expansion ends
	Nozzle exit
	External expansion begins
10	External expansion ends

The impact of vehicle structural vibration to the propulsion system is mainly reflected in: the change of air turning angle due to the structure displacement of the body leading edge:

$$\delta = \alpha + \Delta\delta + \tau_1 \tag{36}$$

Where $\Delta\delta = \arctan[\Phi'(x_0)\eta(t)]$ and τ_1 is the wedge angle of the forward fuselage. Thus the shock angle is changed which affects the engine intake conditions and ultimately the engine thrust, and the additional force and moment.

At the condition of height $h = 25\mathrm{km}$, Mach $Ma = 8$ and elevator angular deflection $\delta_e = 0^\circ$, the thrust coefficient ($0^\circ \le \alpha \le 10^\circ$, $0.2 \le \delta_T \le 1$) is shown in Fig.6. The thrust coefficient is approximately linear with AOA and fuel equivalence ratio (FER). The greater the AOA, the more changes in thrust coefficient with δ_T.

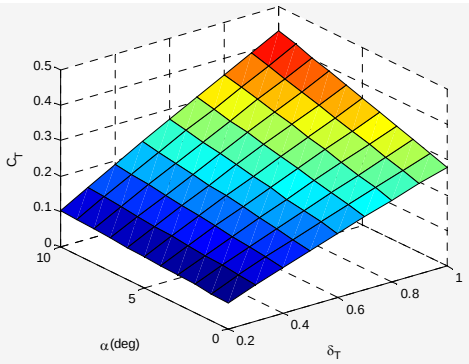

Fig. 6 Thrust coefficient against α and δ_T

Furthermore, with consideration of the first three orders vibration mode, Fig.7 shows the curves of thrust coefficients for the conditions of different Mach and temperature of structure.

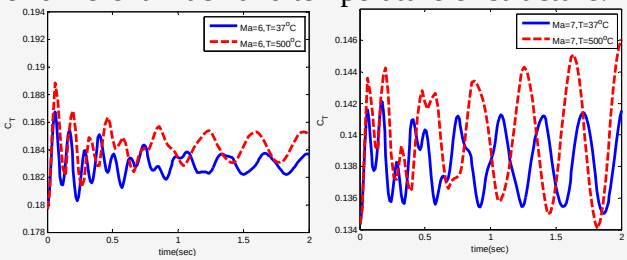

Fig. 7 Thrust coefficient Time-Domain response with Ma 6 and Ma 7

Based on above analysis, we can draw the following conclusions:

(1) When the vehicle is at the altitude of 25km, the divergence Mach number of structure vibration of fuselage is between 6 to 7;

(2) Because the higher order vibration modes have high vibration frequency and fast attenuation, it makes thrust coefficient performs irregular shapes summed by several vibration modes in a very short period of vibration at the early stage. Then it shows the typical first-order modal vibration characteristics. That means the first structure vibration mode is the most important factor affecting the control performance.

(3) When the structure disturbed in the high temperature operating condition, the convergence slows down or, the divergence increases rapidly. It cannot be ignored for control system design.

4 Result of modeling and analysis

Based on above methods, a specific model is obtained at the condition of $h=30km$, $Ma=10$ and $\delta_e=0^\circ$. CFD software is used for validating the results of engineering method. Fig.8 shows the static pressure distribution calculated by CFD software. Fig.9 shows the comparison of two results.

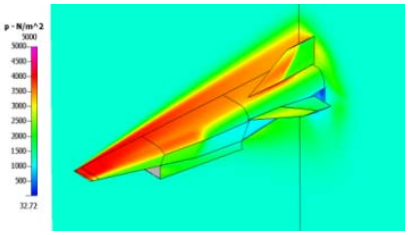

Fig. 8 Static pressure

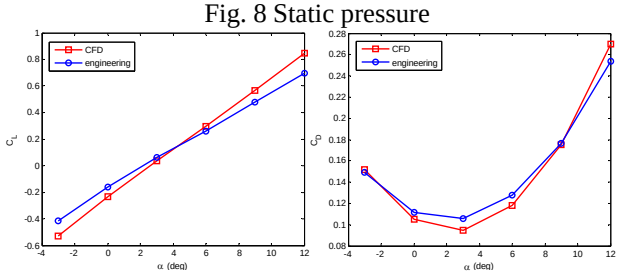

Fig. 9 Contrast of CL、CD against AOA between Engineering and CFD

The typical mission of this vehicle is hypersonic cruise flight, and the directional and lateral motions are not considered. Therefore, this paper only considers the vertical movement. The first elastic mode impacts the rigid body motion mostly. Thus the longitudinal dynamical equations of air-breathing hypersonic vehicle are:

$$\begin{aligned}
\dot{V} &= \frac{1}{m}(T\cos\alpha - D) - g\sin(\theta-\alpha)\\
\dot{\alpha} &= \frac{1}{mV}(-T\sin\alpha - L) + Q + \frac{g}{V}\cos(\theta-\alpha)\\
I_{yy}\dot{Q} &= M_{yy}\\
\dot{\theta} &= Q\\
\dot{h} &= V\sin(\theta-\alpha)\\
\ddot{\eta} &= -2\zeta\omega\dot{\eta} - \omega^2\eta + N
\end{aligned} \tag{37}$$

The thrust T, lift L, drag D, pitching moment M and generalized force N are:

$$\begin{aligned}
T &= qSC_T\\
L &= qSC_L\\
D &= qSC_D\\
M &= qScC_M\\
N &= qSC_N
\end{aligned} \tag{38}$$

Where $q=\frac{1}{2}\rho V^2$ is dynamic pressure, S is reference area, c is mean aerodynamic chord.

The flight height h is 25km, α is AOA, V is velocity, δ_e is elevator angular deflection, δ_T is fuel equivalence ratio, η is generalized elastic coordinate, $\dot{\eta}$ is the derivative of η. The

ranges and intervals of these variables in calculation are shown in Table 3.

Table 3 the range and interval of variables

Variables	Range	Interval
α	[-5°，10°]	5°
Ma	[6,12]	2
δ_e	[-10°，15°]	5°
δ_T	[0.3，0.9]	0.3
η	[-0.2，0.4]	0.2
$\dot{\eta}$	[-2，4]	2

Multivariate fitting method is used to get the fitting formula of the aerodynamic coefficients. In order to ensure the fitting accuracy, vector relative error RE (relative error) is introduced to evaluate the fitting results:

$$RE = \frac{\|\boldsymbol{u}-\hat{\boldsymbol{u}}\|_2}{\|\boldsymbol{u}\|_2}\times 100\% \tag{39}$$

Where $\boldsymbol{u}$ is the actual data vector, $\hat{\boldsymbol{u}}$ is the calculated vector using fitting formula, $\|\bullet\|_2$ is the vector norm.

The lift coefficient C_{L}, drag coefficient C_{D}, pitching moment coefficient C_{M}, thrust coefficient C_{T} and generalized force coefficient C_{N} are:

$$\begin{aligned}
&C_L = 0.2034 - 0.3781Ma + 0.8647\alpha - 0.1443Ma\cdot\alpha + \\
&0.0885\delta_e + 0.1761\delta_T - 0.078\delta_T^2 - 0.0277\eta - 0.0056\dot{\eta} \\
&C_D = 0.142 - 0.0848Ma + 0.0179\alpha + 0.1703\alpha^2 - 0.0711Ma\cdot\alpha + 0.0303\delta_e^2 \\
&C_M = -0.9036 + 1.9841Ma - 0.9423Ma^2 + 0.1934\alpha + 0.1627\alpha^2 + \\
&0.0832Ma\cdot\delta_e - 0.1749\delta_e - 0.0715\delta_e^3 - 0.2871\delta_T + 0.1271\delta_T^2 + 0.05\eta \\
&C_T = 0.9816 - 2.9788Ma + 2.9517Ma^2 - 1.0253Ma^3 + 0.6626\alpha - 1.9155Ma\cdot\alpha + \\
&2.0073Ma^2\cdot\alpha - 0.7272Ma^3\cdot\alpha + 0.1777\delta_T - 0.0117\delta_T^2 + 0.0216\eta \\
&C_N = 0.0009 + 0.7046Ma - 0.3652Ma^2 - 1.6675\alpha + 0.7982\alpha^2 - 0.2537\alpha^3 + \\
&0.2918Ma\cdot\delta_e - 0.4863\delta_e - 0.6043\delta_e^2 - 0.4554\delta_e^3 + 0.2209\eta + 0.0793\dot{\eta}
\end{aligned} \tag{40}$$

The fitting errors were 7.81%，6.17%，17.95%，12.68%，21.84% respectively. It can be used for guidance and control law design and simulation.

With constraints of mass flow, dynamic pressure and fuel equivalence ratio, the engine envelope is shown in fig.10.

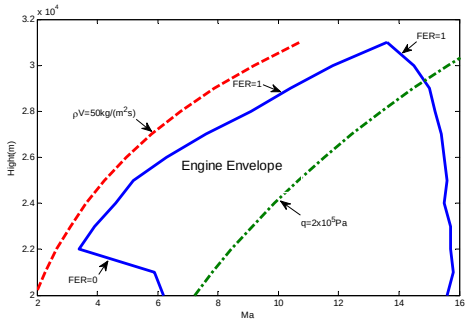

Fig.10 Scramjet-Powered Engine Envelope

In the envelope of Scramjet-Powered Engine, trim analysis is shown for AOA, elevator deflection, FER and L/D respectively at different altitudes (Fig.11-14).

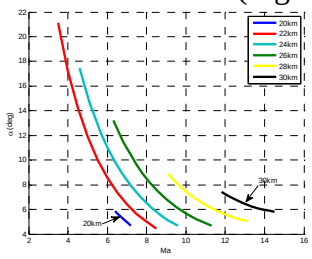

Fig.11 Trim AOA

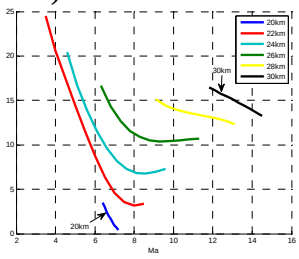

Fig.12 Trim Elevator Deflection

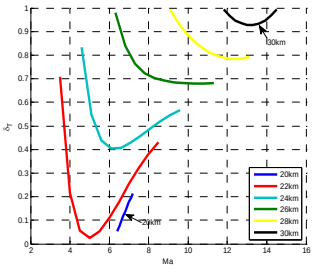

Fig.13 Trim FER

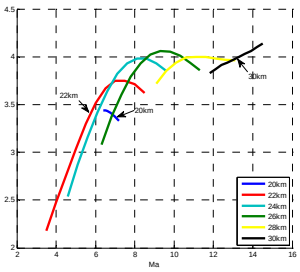

Fig.14 Trim L/D

After analysis, we can draw the following conclusions:

(1) The value of trim AOA is proportional to the flight height and inversely proportional to Mach. As flight altitude increases, atmospheric density decreases, then the atmospheric pressure decreases, so the lift of vehicle is getting smaller. In order to counteract gravity, it must increase the AOA to increase lift. In another way, at the same height, the greater Mach is, the greater dynamic pressure is. And the lift value is proportional to the dynamic pressure. Therefore, in order to maintain the cruise height, the AOA must to be reduced to get the proper lift to balance against gravity.

(2) Trim elevator angular deflection and trim AOA is broadly similar trend with altitudes and Mach. The stable cruise flight of vehicle requires the pitching moment to be zero. Generally, the positive AOA causes upward

force moment, and an elevator angular deflection is needed to produce downward force moment to offset it. Therefore, usually a large trim AOA is corresponding to a large trim elevator angular deflection. In addition, elevator angular deflection plays a very important role on the stability of structure vibration for the flexible body vehicle.

(3) It can be seen from the fitting formula of the thrust coefficient that except for fuel-to-air ratio, AOA and Mach are the mainly factors to decide thrust value of scramjet. The thrust coefficient is proportional to AOA, and inversely proportional to Mach. The increase of flight Mach, and the decrease the trim AOA, will result in decrease of thrust. Since the cruise flight requires $T\cos\alpha = D$, the trim δ_T must increase. On the other hand, the large trim AOA means large drag, and thrust components in the opposite direction of drag will be smaller. So the trim δ_T must be increased to balance the drag. This is the reason of the trim δ_T decreases and then increases with Mach in fig.13. Similarly, with the increase of flight altitude, the atmospheric density decreases. It will require increased trim δ_T to provide thrust.

(4) In fig.14, the lift-drag ratios of vehicle are between 3.5 to 4. The vehicle has good flight trimming performances as a wave-rider hypersonic vehicle.

5 Dynamic analysis

The pole-zero point analysis is one of the important means for flight control analysis. The pole-point shows the dynamic stability of vehicle in certain flight conditions, while the zero-point shows the weight of corresponding modal.

Linearized at the trim condition of Mach 8 and altitude 25km, the open-loop poles of the linearized dynamics are: -0.87±19.59i，-1.8381，1.8124，-4.45×10^{-4}，-1.2×10^{-5}±0.0376. The vehicle has an unstable short period mode and a stable phugoid mode. The altitude mode is stable, although it is a very slow mode. The aero elastic mode is a pair of stable complex-conjugate poles. In the following analysis of pole-zero point, the input of system is elevator angular deflection; output of system is flight path angle (FPA).

Fig.15 shows the pole-zero point changes with Mach 8 and altitude between 22km to 26km. The system is unstable and non-minimum phase. The instability is due to the mass center behind the pressure center, which results in a pitch up instability. The right half plane (RHP) transmission zero is associated with the elevator to FPA map. When the elevator is deflected upward, the vehicle loses altitude before it climbs.

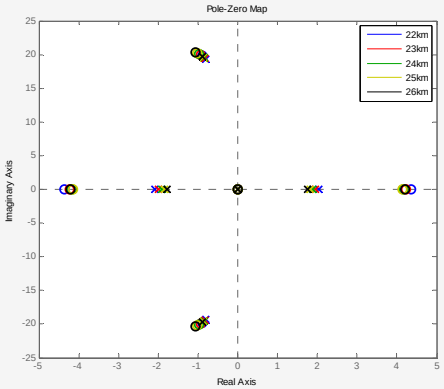

Fig. 15 pole-zero point changes with altitude

At all flight conditions, the vehicle has a real unstable pole and a stable (short period mode) pole whose absolute value are almost the same. As the altitude increases, these poles are observed to move toward the origin. The vehicle becomes more stable when altitude is increasing. It implies that the vehicle will require a larger bandwidth for stabilization at lower altitude. The zeros are also observed to move toward the origin when altitude is increasing. At higher altitudes, the RHP zeros moves closer to the origin. From control perspective, the RHP zeros will require large deflection of elevator at higher altitude.

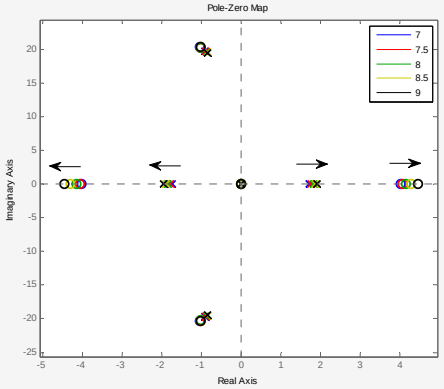

Fig 16 pole-zero point changes with Mach

Fig.16 shows the pole-zero points with altitude 25km and Mach between 7 to 9. As the Mach increases, the poles are observed to move away from the origin. Hence, the vehicle becomes less stable with Mach increasing. It implies that the vehicle will require a larger bandwidth for stabilization at larger speed. Real zeros which are symmetric with respect to the imaginary axis are observed to move away from the origin when Mach increases. The RHP zeros will require large deflection of elevator at lower Mach number.

The mode sensitivity analysis method is used to study mode sensitivity for each flight state and determine the primary contribution of each flight state to each movement mode.

Table 4 the sensitivities of modes to flight states

State	*AE*	*SP*	*SP*	*LP*	*LP*
V	0	0.0003	0.0003	0.4997	0.4997
α	0.0005	0.5027	0.4963	0	0
Q	0.0005	0.4957	0.5033	0	0
γ	0	0	0	0.5	0.5
η	0.4995	0.0002	0.0008	0	0
$\dot{\eta}$	0.4995	0.0005	0.0005	0	0

Analysis of the mode sensitivity (table 4) tells that the most significant contributions for the phugoid mode are velocity V and FPA γ. The short period mode is dominated by AOA α and the pitching angular rate Q. In addition, the states of the first order structure bending η and $\dot{\eta}$ also make a weak contribution. It can be seen that band separation exists between the phugoid mode and the short period mode. At the same time, there are small cross-coupling between the rigid body dynamics and structural dynamics.

Table 5 the sensitivities of modes to flight states with low frequency of fuselage vibration

State	*AE*	*SP*	*SP*	*LP*	*LP*
V	0.0005	0.0005	0.0005	0.552	0.4458
α	0.2501	0.2499	0.2499	0	0
Q	0.2483	0.2517	0.2517	0	0
γ	0	0	0	0.4468	0.5532
η	0.2455	0.2545	0.2545	0	0
$\dot{\eta}$	0.2544	0.2456	0.2456	0	0

The table 5 shows the mode sensitivity when the frequency of fuselage vibration is 2Hz. The contributions of state α, Q, η and $\dot{\eta}$ for short period mode and aero elastic mode are almost equal. The difficulty to control the vehicle will increase rapidly with the lower frequency of the structure natural vibration.

Conclusions

This paper combines with parameterized configuration approach, engineering calculated method of aerodynamic, aero-thermal and the thrust and elastic assumptions of the fuselage to establish a multi-field coupling model for wave-rider air-breathing hypersonic vehicle. Through calculation and analysis, the conclusions are:

(1) The viscous drag generated by the boundary layer temperature cannot be ignored when calculating the aerodynamic forces.

(2) High temperature causes the change of structural materials performance which will result in elastic vibration of fuselage. The elastic vibration will affect thrust value of scramjet significantly.

(3) In this paper, the difference between results of the selected method of aerodynamic engineering calculation and CFD method are small.

(4) This nonlinear model of hypersonic vehicle has good flight trimming performance. It can be used for flight control law design and simulation analysis.

References

[1] Jeffrey J.Dickeson, Armando A.Rodriguez, Srikanth Sridharan, et al. Decentralized control of an air-breathing scramjet-powered hypersonic vehicle[R]. AIAA 2009-6281, 2009.

[2] John, D. Shaughnessy, S. Zane Pinckey, John D. Mc Minn, et al. Hypersonic vehicle simulation model: wi nged-cone configuration[R]. NASA TM 102610, 199 0.

[3] Martin R. Waszak, David K. Schmit. On the flight dynamics of aeroelastic vehicles[C]. AIAA-1986-2077-388,1986.

[4] Martin R. Waszak, David K. Schmit. Flight dynamics of aero-elastic vehicles[J]. Aircraft 1988,25(6):563-571.

[5] Karl D. Bilimoria, David K. Schmit. Integrated development of the equations of motion for elastic hypersonic flight vehicles[J]. Guidance, control and dynamics. 1995,18(1):73-81.

[6] Frank R. Chavez, David K. Schmit. Analytical aeropropulsive/aeroelastic hypersonic-vehicle model with dynamic analysis[J]. Guidance, control and dynamics. 1994,17(6):1308-1319.

[7] Bolender M A, Doman D B. A non-linear model for t he longitudinal dynamics of a hypersonic air-breathin g vehicle[R]. AIAA-2005-6255,2005.

[8] Jason T.Parker, Bolender M A, Doman D B. Control-oriented modeling of an air-breathing hypersonic vehicle[J]. Guidance, control and dynamics. 2007, 30(3): 856-869.
[9] Trevor Williams, Bolender M A. An aerothermal flexible mode analysis of a hypersonic vehicle[C]. AIAA-2006-6647.
[10] Bolender M A, David B. Doman. Modeling unsteady heating effects on the structural dynamics of a hypersonic vehicle[C]. AIAA-2006-6646.
[11] Adam J. Culler, Trevor Williams. Aerothermal modeling and dynamic analysis of a hypersonic vehicle[C]. AIAA-2007-6395.
[12] J. E. Gregoire, R. J. Krieger. Aerodynamic Prediction Rationale for Advanced Arbitrarily Shaped Missile Concepts[R]. AIAA-80-0256, 1980
[13] Moore M, Williams J. Aerodynamic Prediction Rationale for Analyses of Hypersonic Configurations[R]. AIAA-89-0525, 1989.
[14] Vosteen, L.F. Effect of temperature on dynamic modulus of elasticity of some structural alloys[R]. NACA technical note, august 1958, NACA TN 4348.
[15] Amando A.Rodriguez, Jeffrey J.Dickeson, etc. Control-relevant modeling, analysis, and design for scramjet-powered hypersonic vehicles[C]. AIAA-2009-7287-980.
[16] William H.Heiser, David T.Pratt. Hypersonic air-breathing propulsion [M]. AIAA Education Series. 1994.
[17] Anderson, John David. Modern compressible flow [M]. Boston: McGraw-Hill, 2003.

Copyright Statement